Electronic Supplementary Material (ESI) for ChemComm.

Long-lived, near-IR emission from Cr(III) under ambient conditions

Natalia Sawicka,[a] Chloe J. Craze,[a] Peter N. Horton,[b] Simon J. Coles,[b]
Emma Richards,*[a] and Simon J.A. Pope*[a]

[a]School of Chemistry, Main Building, Cardiff University, Cardiff CF10 3AT, Cymru/Wales, UK; [b]UK National Crystallographic Service, Chemistry, Faculty of Natural and Environmental Sciences, University of Southampton, Highfield, Southampton, SO17 1BJ, England, UK.
Email: richardse10@cardiff.ac.uk, popesj@cardiff.ac.uk

Electronic Supplementary Information

Table of Contents

Experimental

All reactions were performed with the use of vacuum line and Schlenk techniques. Reagents were commercial grade and were used without further purification. ^{1}H and $^{13}C\{^{1}H\}$ NMR spectra were recorded on a Bruker Avance dpx 400, or Bruker Avance dpx 500 MHz spectrometer and were recorded in $CDCl_3$. ^{1}H and $^{13}C\{^{1}H\}$ NMR chemical shifts (δ) were determined relative to internal tetramethylsilane, $Si(CH_3)_4$ and are given in ppm. Low- and high-resolution mass spectra were obtained by the staff at Cardiff University. All photophysical data was obtained on a JobinYvon-Horiba Fluorolog-3 spectrometer fitted with a Hamamatsu R5509-73 detector (cooled to –80 °C using a C9940 housing) was used for near-IR luminescence measurements. For the near-IR lifetimes the pulsed laser source was a Continuum Minilite Nd:YAG configured for 355 nm output. Luminescence lifetime profiles were obtained using the JobinYvon–Horiba FluoroHub single photon counting module and the data fits yielded the lifetime values using the provided DAS6 deconvolution software. IR spectra were recorded on an ATR equipped Shimadzu IRAffinity-1 spectrophotometer. UV-vis data were recorded as solutions on a Perkin Elmer Lamda20 spectrophotometer. HPLC purification was conducted using a Waters Synapt G2 SI using a water aceonitrile solvent gradient.

X-ray crystallography

Data collection and processing

A suitable crystal of $[Cr(\textbf{bpi-1})_2]PF_6$ was selected and data collected on a Rigaku 007HF diffractometer equipped with HF Varimax confocal mirrors, an AFC11 goniometer and HyPix 6000HE detector. Cell determination, data collection, data reduction, cell refinement and absorption correction were carried out using CrysAlisPro.[1] The structure was solved with ShelXT [2] by using Olex2 [3] as the graphical interface. The model was refined with version 2018/3 of ShelXL [4] using Least Squares minimisation. All non-hydrogen atoms were refined anisotropically. Hydrogen atom positions were calculated geometrically and refined using the riding model. For $[Cr(\textbf{bpi-1})_2]PF_6$, the crystal used was a non-merohedral twin; the solvent ether was disordered over a symmetry operator, resulting in the use of displacement (RIGU) restraints. CCDC 2155916 contains supplementary X-ray crystallographic data for $[Cr(\textbf{bpi-1})_2]PF_6$. This data can be obtained free of charge via http://www.ccdc.cam.ac.uk/conts/retrieving.html, or from the Cambridge

Crystallographic Data Centre, Union Road, Cambridge, CB2 1EZ; fax(+44) 1223-336-033 or email: deposit@ccdc.cam.ac.uk.

EPR Spectroscopy

Samples for EPR measurements were prepared in MeCN solvent under atmospheric conditions. The X-band CW EPR measurements were performed on a Bruker EMX spectrometer utilizing an ER4119HS resonator, 100 kHz field modulation and 0.4 mT modulation depth at 140 K. Additional high-frequency measurements were performed on a Bruker Elexsys E680 spectrometer, operating at ~ 94 GHz. Measurements were recorded at both 298 K and 20 K with application of an Oxford Instruments liquid-helium cryostat, using a Bruker ER5106 QT-E Q-band resonator. Spectrometer conditions utilized 100 kHz field modulation, 10 G modulation depth, 81.92 ms conversion time and 0.01581 mW microwave power. EPR simulations were performed using the Easyspin toolbox within Matlab. [5]

Experimental

Experimental

Synthesis of di(pyridin-2-yl)isoindoline-1,3-diimine (Hbpi-1)

Phthalonitrile (0.334 g, 2.61 mmol), 2-aminopyridine (0.492 g, 5.23 mmol) and $CaCl_2$ (0.065 g, 0.582 mmol) were stirred at reflux in *n*-butanol for 48 hr. Upon cooling, yellow needle-like crystals were observed and subsequently filtered followed by washing with water to afford the product (0.453 g, 58 %). ^{1}H NMR (500 MHz, $CDCl_3$): δ_H 13.99 (s, 1H), 8.61 (ddd, *J* = 4.9, 2.0, 0.9 Hz, 2H), 8.11 – 8.04 (m, 2H), 7.76 (ddd, *J* = 8.1, 7.4, 2.0 Hz, 2H), 7.68 – 7.61 (m, 2H), 7.46 (dt, *J* = 8.0, 1.0 Hz, 2H), 7.11 (ddd, *J* = 7.4, 4.9, 1.1 Hz, 2H) ppm; $^{13}C\{^1H\}$ NMR (126 MHz, $CDCl_3$): δ_C 160.6, 153.9, 147.9, 138.2, 135.9, 131.8, 123.3, 122.7, 120.3 ppm. IR (solid): ν 3111 w, 2980, 1628, 1581, 1570, 1456, 1458, 1377, 1259, 1221, 1144, 1097, 1036, 966, 767, 698 s, 524 s, 401 cm^{-1}. UV-Vis (MeCN) λ_{max} (ε, $M^{-1}cm^{-1}$): 235 (32000), 275 (15600), 285(15400), 289 (15300), 315 (9100), 330 (10900), 345 (11900), 356 (14200), 380 (15100), 405 (9200) nm. LRMS (ES+): *m/z* 300.13 $[M+H]^+$ for $C_{18}H_{13}N_5$.

Synthesis of di(4-ethylpyridin-2-yl)isoindoline-1,3-diimine (Hbpi-2)

As for **Hbpi-1** but using phthalonitrile (0.323 g, 2.52 mmol), 4-ethylpyridin-2-amine (0.649 g, 5.31 mmol) and $CaCl_2$ (0.050 g, 0.450 mmol) giving the product (0.539 g, 61%).^{1}H NMR (500 MHz, $CDCl_3$): δ_H 13.99 (s, 1H), 8.49 (dd, *J* = 5.1, 0.7 Hz, 2H), 8.07 (dd, *J* = 5.6, 3.1 Hz, 2H), 7.64 (dd, *J* = 5.6, 3.1 Hz, 2H), 7.35 – 7.29 (m, 2H), 7.00 – 6.94 (m, 2H), 2.70 (q, *J* = 7.6 Hz, 4H), 1.30 (t, *J* = 7.6 Hz, 6H) ppm; $^{13}C\{^1H\}$ NMR (126 MHz, $CDCl_3$): δ_C 160.7, 155.4, 153.9, 147.7, 135.9, 133.7, 133.3, 131.7, 122.7, 122.5, 120.4, 28.4, 14.5 ppm. IR (solid): ν 3240 w, 1647, 1628, 1589, 1582, 1466. 1452, 1406, 1302, 1244, 1101, 1042, 893, 841, 777, 691, 457, 419 cm^{-1}. UV-Vis (MeCN) λ_{max} (ε, $M^{-1}cm^{-1}$): 230 (30700), 275 (17100), 285 (16800), 295 (15900), 315 (11000), 330 (13500), 345 (15200), 365 (18400), 385 (19900), 405 (9200). HRMS: found *m/z* 356.1874 $[M+H]^+$, calculated *m/z* for $[C_{22}H_{22}N_5]^+$ is 356.1874.

Synthesis of $[Cr(bpi\text{-}1)_2]PF_6$

Di(pyridin-2-yl)isoindoline-1,3-diimine (0.295 g, 0.988 mmol) and $CrCl_3(THF)_3$ (0.185 g, 0.494 mmol) were stirred under reflux in dry ethanol for 24h. Upon cooling, the dark brown solution was filtered to obtain a brown precipitate and red-brown filtrate. NH_4PF_6 was added in excess to the red-brown ethanol solution resulting in red-brown precipitate which was subsequently filtered and washed with diethyl ether. The complex was purified using HPLC using a water / MeCN solvent gradient. (0.043 g, 19%). IR (solid) ν 3344 w, 1645, 1578, 1533, 1468, 1433, 1285, 1196, 1089, 835 (PF_6), 773, 718, 557 (PF_6), 518 cm^{-1}. UV-Vis (MeCN) λ_{max} (ε, $M^{-1}cm^{-1}$): 234 (18700), 256 (13800), 293 sh (4400), 320 sh (7000), 354 sh (8300), 380 (8300), 412 sh (5500), 464 (5700), 490 (6200), 607 (90), 699 (10), 750 (6), 825 (1) nm. HRMS: found *m/z* 648.1589, calculated *m/z* for $[C_{36}H_{24}N_{10}{}^{52}Cr]^+$ is 648.1591.

Synthesis of $[Cr(bpi\text{-}2)_2]PF_6$

Di(4-ethylpyridin-2-yl)isoindoline-1,3-diimine (0.501 g, 1.410 mmol) and $CrCl_3(THF)_3$ (0.254 g, 0.678 mmol) were stirred in dry ethanol for 24h under reflux. After cooling the resultant red-brown solution was filtered under vacuum. Subsequently, NH_4PF_6 was added to the filtrate resulting in a precipitation of a red-brown solid which was

filtered and washed with diethyl ether to obtain the crude product (0.612 g, 59%). The complex was purified using HPLC using a water / MeCN solvent gradient. IR (solid) ν 3395 w, 2986 s, 1724, 1630, 1582, 1522, 1474, 1416, 1381, 1298, 1190, 1084, 833 s (PF_6), 718, 555 s (PF_6) cm^{-1}. UV-Vis (MeCN) λ_{max} (ε, $M^{-1}cm^{-1}$): 242 (28300), 282 (17400), 335 (10200), 353 (9400), 377 (8300), 411 (6800), 459 (6200), 483 (6100), 752 (9), 840 (9) nm. HRMS: found *m/z* 760.2860, calculated *m/z* for $[C_{44}H_{40}N_{10}{}^{52}Cr]^+$ is 760.2843.

Table S1. The data collection parameters associated with the crystallographic studies on [Cr(**bpi-1**)$_2$]PF$_6$.

Compound	**[Cr(bpi-1)$_2$]PF$_6$**
Formula	$C_{38}H_{29}CrF_6N_{10}O_{0.5}P$
$D_{calc.}$/ g cm^{-3}	1.560
m/mm^{-1}	3.787
Formula Weight	830.68
Colour	red
Shape	needle-shaped
Size/mm^3	0.14×0.02×0.01
T/K	100(2)
Crystal System	monoclinic
Space Group	$P2_1/n$
a/Å	12.2896(3)
b/Å	8.7251(2)
c/Å	32.9959(10)
α/°	90
β/°	91.483(2)
γ/°	90
V/Å^3	3536.90(16)
Z	4
Z'	1
Wavelength/Å	1.54178
Radiation type	Cu Kα
Θ_{min}/°	2.679
Θ_{max}/°	70.606
Measured Refl's.	9714
Indep't Refl's	9714
Refl's I≥2 σ(I)	7915
R_{int}	.
Parameters	535
Restraints	21
Largest Peak	1.913
Deepest Hole	-0.677
GooF	1.050
wR_2 (all data)	0.2576
wR_2	0.2486
R_1 (all data)	0.1038
R_1	0.0894

Table S2. Selected bond lengths and bond angles obtained from crystallographic data for [Cr(**bpi-1**)$_2$]PF_6.

Compound: [Cr(bpi-1)$_2$]PF_6					
			XRD	**DFT – Ground State**	**DFT – Excited State**
Bond Lengths (Å)					
Cr1		N1	2.097(6)	2.140	2.129
Cr1		N3	1.993(6)	2.010	1.955
Cr1		N5	2.088(6)	2.140	2.128
Cr1		N21	2.107(6)	2.140	2.128
Cr1		N23	1.986(6)	2.010	1.955
Cr1		N25	2.098(6)	2.140	2.129
Bond Angles (°)					
N1	Cr1	N5	172.8(2)	173.97	172.99
N21	Cr1	N25	173.5(2)	173.97	172.97
N23	Cr1	N3	175.6(2)	179.98	179.99
N23	Cr1	N21	87.8(2)	86.98	86.48
N23	Cr1	N1	91.0(2)	93.00	93.50
N23	Cr1	N25	86.1(2)	86.99	86.49
N23	Cr1	N5	95.6(2)	93.03	93.51
N3	Cr1	N21	95.7(2)	93.00	93.53
N3	Cr1	N1	86.2(2)	86.99	86.49
N3	Cr1	N25	90.5(2)	93.02	93.50
N3	Cr1	N5	87.4(2)	86.99	86.49
N1	Cr1	N25	90.4(2)	91.25	93.06
N25	Cr1	N5	92.9(2)	89.04	87.35
N5	Cr1	N21	85.3(2)	91.25	93.11
N11	Cr1	N1	92.1(2)	89.09	87.34

Table S3 Selected bond lengths and angles of Cr(III) systems

Bond Lengths (Å)				**Bond Angles (°)**			
Cr(tpy)Cl_3							
Cr–N	2.068	Cr–Cl	2.338	N_{py}-Cr-N_{py}	78.25	N_{py}-Cr-Cl	87.86
Cr–N	2.067	Cr–Cl	2.327	N_{py}-Cr-N_{py}	88.08	N_{py}-Cr-Cl	86.62
Cr–N	1.990	Cr–Cl	2.298	N_{py}-Cr-N_{py}	78.23	N_{py}-Cr-Cl	102.17
				Cl-Cr-Cl	93.53	N_{py}-Cr-Cl	101.37
				Cl-Cr-Cl	92.78		
Cr(acac)$_3$							
Cr–O1	1.967	Cr–O4	1.958	O1–Cr–O2	90.78	O1–Cr–O3	90.14
Cr–O2	1.695	Cr–O5	1.948	O2–Cr–O3	88.22	O3–Cr–O4	91.47
Cr–O3	1.964	Cr–O6	1.955	O2–Cr–O4	89.53	O4–Cr–O6	88.85
				O2–Cr–O6	91.18	O6–Cr–O1	89.55
				O1–Cr–O5	90.18	O4–Cr–O5	89.58
				O3–Cr–O5	89.23	O6–Cr–O5	91.37
Mer-$CrCl_3(pzH)_3$							
Cr–N1	2.072	Cr–Cl1	2.323	N1-Cr-N3	87.93	Cl1-Cr-Cl2	90.65
Cr–N1a	2.072	Cr–Cl1a	2.323	N1-Cr-Cl1	89.40	NCl2-Cr-Cl1a	90.65
Cr–N3	2.092	Cr–Cl2	2.324	N1-Cr-Cl2	92.07	Cl1a-Cr-N3	89.35
				N1-Cr-Cl1a	90.55	N3-Cr-Cl1	89.35
				N1a-Cr-N3	87.93	N1a-Cr-Cl2	92.07
				N1a-Cr-Cl1	90.55	N1a-Cr-Cl1a	89.40

Cartesian Coordinates

Cartesian Coordinates for ground state [Cr(**bpi-1**)$_2$]PF_6 determined from XRD measurements.

```
Cr 5.95068 6.44846 11.92699
N 7.08354 7.43030 13.39383
N 8.38707 5.51601 14.12114
N 7.34855 5.02828 11.98702
N 6.83185 3.76139 10.01387
N 5.04750 5.36070 10.38990
N 6.84700 7.56030 10.37802
N 5.03366 0.41270 10.02245
N 4.54938 7.85259 12.01902
N 3.59117 7.38754 14.18777
N 4.85484 5.45755 13.41692
C 6.86831 0.03839 13.58976
H 6.37406 0.51090 12.93089
C 7.32286 0.74687 14.68815
H 7.11102 1.66645 14.80109
C 8.10112 0.06806 15.62492
H 8.40436 0.50497 16.41326
C 8.41942 7.48177 15.38743
H 8.98657 7.02096 15.99300
C 7.92615 6.81169 14.26595
C 8.19073 4.79531 13.06530
C 8.89311 3.49702 12.85090
C 9.81862 2.83129 13.60625
H 10.10460 3.16840 14.44654
C 10.33344 1.62636 13.08839
H 10.98566 1.14320 13.58283
C 9.88889 1.12728 11.84156
H 10.25262 0.31807 11.50284
C 8.92107 1.81133 11.10600
H 8.59469 1.47076 10.28256
C 8.45147 3.01801 11.63376
C 7.46353 3.97516 11.10600
C 5.69713 4.45329 9.60189
C 5.19481 4.10429 8.35506
H 5.69823 3.52771 7.79125
C 3.98203 4.57893 7.91966
H 3.65419 4.35965 7.05592
C 3.24335 5.38862 8.77727
H 2.37212 5.68152 8.53889
C 3.80339 5.75508 9.97792
H 3.29787 6.31428 10.55683
C 8.05768 7.16505 9.94493
H 8.57079 6.59542 10.50590
C 8.59404 7.53936 8.73769
H 9.45862 7.24148 8.48040
C 7.86089 8.35167 7.90977
```

H 8.19145 8.57683 7.04899
C 6.65927 0.10994 8.32538
H 6.15764 0.69130 7.76711
C 6.16159 8.45986 9.60519
C 4.41574 0.18584 11.15218
C 3.43540 1.14124 11.66014
C 2.93802 2.34356 11.17197
H 3.23684 2.69476 10.34266
C 1.99543 3.01801 11.93062
H 1.63279 3.83595 11.61116
C 1.56637 2.49974 13.17085
H 0.91046 2.97099 13.67080
C 2.08298 1.32011 13.67552
H 1.80534 0.98438 14.51967
C 3.01705 0.64566 12.91357
C 3.73562 8.09951 13.11807
C 4.05567 6.10670 14.33192
C 3.64244 5.42963 15.48309
H 3.14609 5.90222 16.14090
C 3.92709 4.11737 15.69089
H 3.66038 3.67910 16.49124
C 4.63415 3.42198 14.67826
H 4.80196 2.48979 14.75317
C 5.06517 4.12697 13.59965
H 5.54642 3.65851 12.92712
P -0.20263 6.46006 11.77625
F 0.86625 6.08227 12.87102
F 11.54117 4.97418 11.77229
F 0.84164 6.03166 10.64091
F 0.31345 7.94159 11.72281
F 11.00789 6.87189 12.86079
F 11.03533 6.83001 10.61419
O 11.66290 6.54557 16.70683
C -0.22060 7.61701 15.87891
H 11.53166 7.61522 15.04835
H 0.73110 7.50266 15.63248
C -0.40564 0.22685 16.61777
H -0.13712 0.96285 16.03014
H 0.14262 0.23255 17.42639
H 10.93832 0.33380 16.86152
C 11.85449 5.28741 16.04713
H 0.52075 5.17009 15.81844
H 11.33015 5.26418 15.20908
C 11.43279 4.21422 16.90803
H 11.36925 3.38373 16.38753
H 10.55643 4.42587 17.28993
H -0.20430 4.09609 17.62885

Cartesian Coordinates for excited state [Cr(**bpi-1**)$_2$]PF_6 determined from TD-DFT calculations. Optimised geometry coordinates from the ground state were taken as the starting point for the excited state geometry.

C	-4.17760	-0.64681	0.26085
C	-4.17772	0.64718	-0.26123
C	-2.77330	1.03018	-0.47310
N	-1.95469	0.00047	-0.00003
C	-2.77311	-1.02950	0.47291
C	-5.36428	1.31803	-0.53427
C	-6.55830	0.65049	-0.26196
C	-6.55818	-0.65068	0.26141
C	-5.36402	-1.31793	0.53382
H	-7.50306	-1.14313	0.45814
H	-5.35761	-2.32118	0.94090
H	-5.35810	2.32129	-0.94133
H	-7.50328	1.14272	-0.45878
N	-2.43927	-2.11889	1.07530
C	-1.19017	-2.38362	1.58954
N	-0.13030	-1.53912	1.46446
C	-1.09918	-3.54799	2.37568
C	0.04366	-3.81224	3.10275
C	1.08644	-2.88640	3.05474
C	0.95586	-1.78240	2.23272
H	-1.96645	-4.19247	2.41367
H	0.11539	-4.70239	3.71549
H	1.99309	-3.01724	3.62996
H	1.75461	-1.06050	2.16910
C	-0.95582	1.78342	2.23201
N	0.13050	1.53976	1.46411
C	-1.08616	2.88730	3.05425
C	-0.04292	3.81257	3.10290
C	1.10001	3.54797	2.37611
C	1.19065	2.38383	1.58959
H	-1.99298	3.01847	3.62913
H	-0.11440	4.70258	3.71588
H	1.96756	4.19204	2.41456
Cr	0.00005	0.00016	-0.00022
N	1.95466	-0.00032	-0.00001
C	2.77334	1.02957	0.47279
C	2.77307	-1.03028	-0.47300
C	4.17773	0.64665	0.26046
C	4.17756	-0.64742	-0.26141
C	5.36432	1.31766	0.53304
C	6.55831	0.65018	0.26050
C	6.55814	-0.65111	-0.26261
C	5.36397	-1.31851	-0.53456
H	5.35815	2.32099	0.93991
H	7.50331	1.14253	0.45692
H	7.50302	-1.14350	-0.45951
H	5.35752	-2.32184	-0.94143

N	2.43906	-2.11969	-1.07526
C	1.18978	-2.38442	-1.58896
C	1.09833	-3.54902	-2.37476
N	0.13003	-1.53975	-1.46379
C	-0.04466	-3.81317	-3.10159
C	-0.95633	-1.78297	-2.23182
C	-1.08726	-2.88712	-3.05357
H	-1.99409	-3.01791	-3.62851
H	-0.11669	-4.70347	-3.71408
H	-1.75493	-1.06091	-2.16821
C	0.95603	1.78294	-2.23192
C	1.08690	2.88691	-3.05389
N	-0.13043	1.53971	-1.46396
C	-1.19023	2.38425	-1.58940
C	-1.09897	3.54853	-2.37569
C	0.04412	3.81277	-3.10233
H	0.11610	4.70291	-3.71504
H	1.99378	3.01774	-3.62875
H	-1.96620	4.19304	-2.41401
N	-2.43949	2.11955	-1.07559
N	2.43973	2.11889	1.07538
H	1.96550	-4.19364	-2.41287
H	-1.75485	1.06190	2.16802
H	1.75476	1.06104	-2.16798

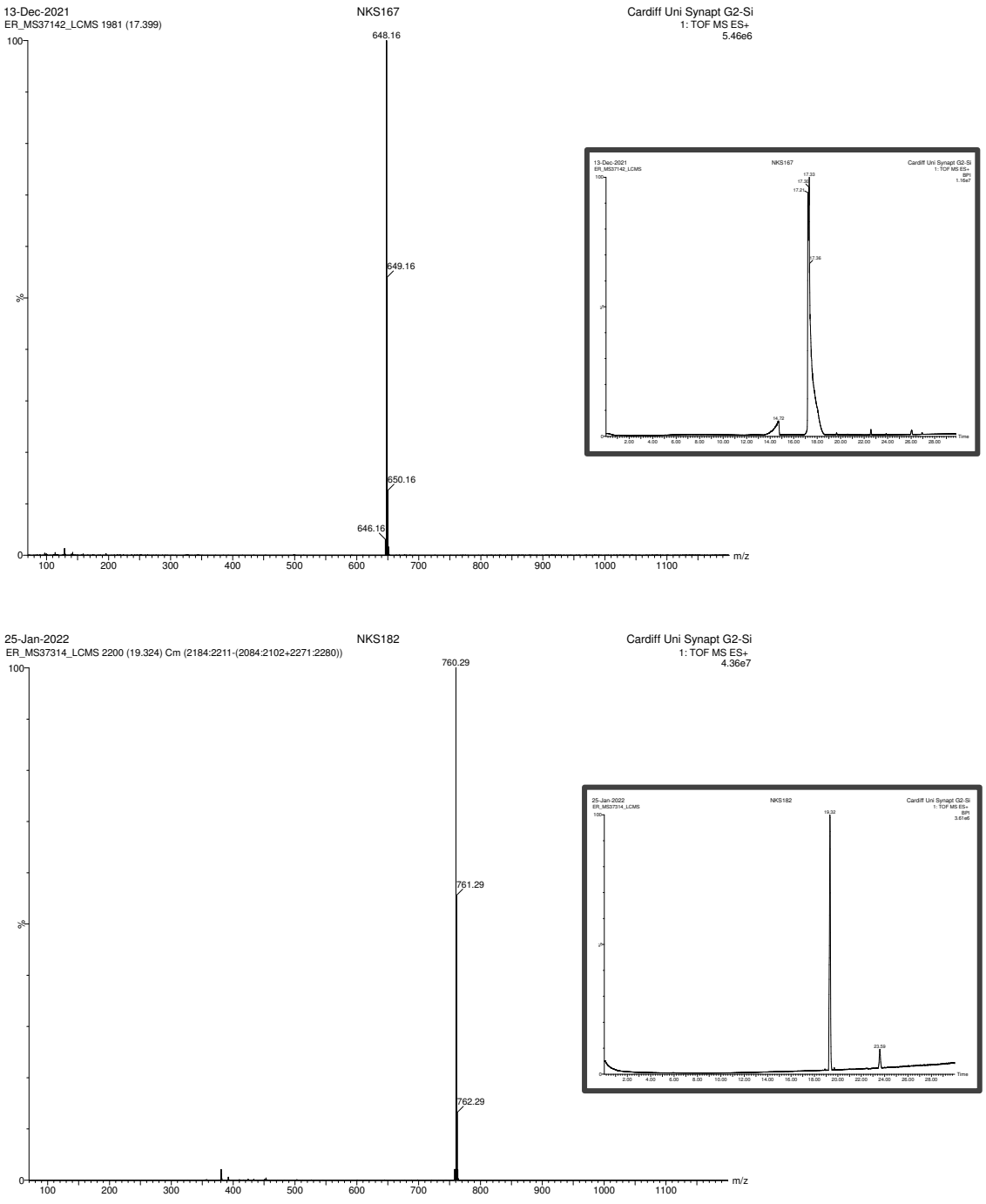

Figure S1 HRMS data from the purified complexes [Cr(**bpi-1**)$_2$]PF_6 (top) and [Cr(**bpi-2**)$_2$]PF_6 (bottom). HPLC chromatograms of the crude complexes shown inset – the dominant peak relates to the pure complex.

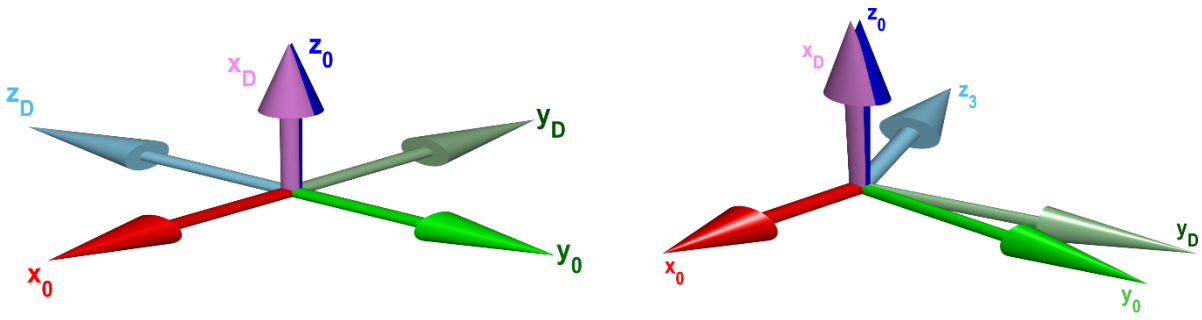

Figure S2 Euler angle rotation of the D-tensor principal axis $(x,y,z)_D$ with respect to the molecular frame $(x,y,z)_0$, for [Cr(**bpi-1**)$_2$]PF_6 (left) and [Cr(**bpi-2**)$_2$]PF_6 (right) as determined by DFT calculations.

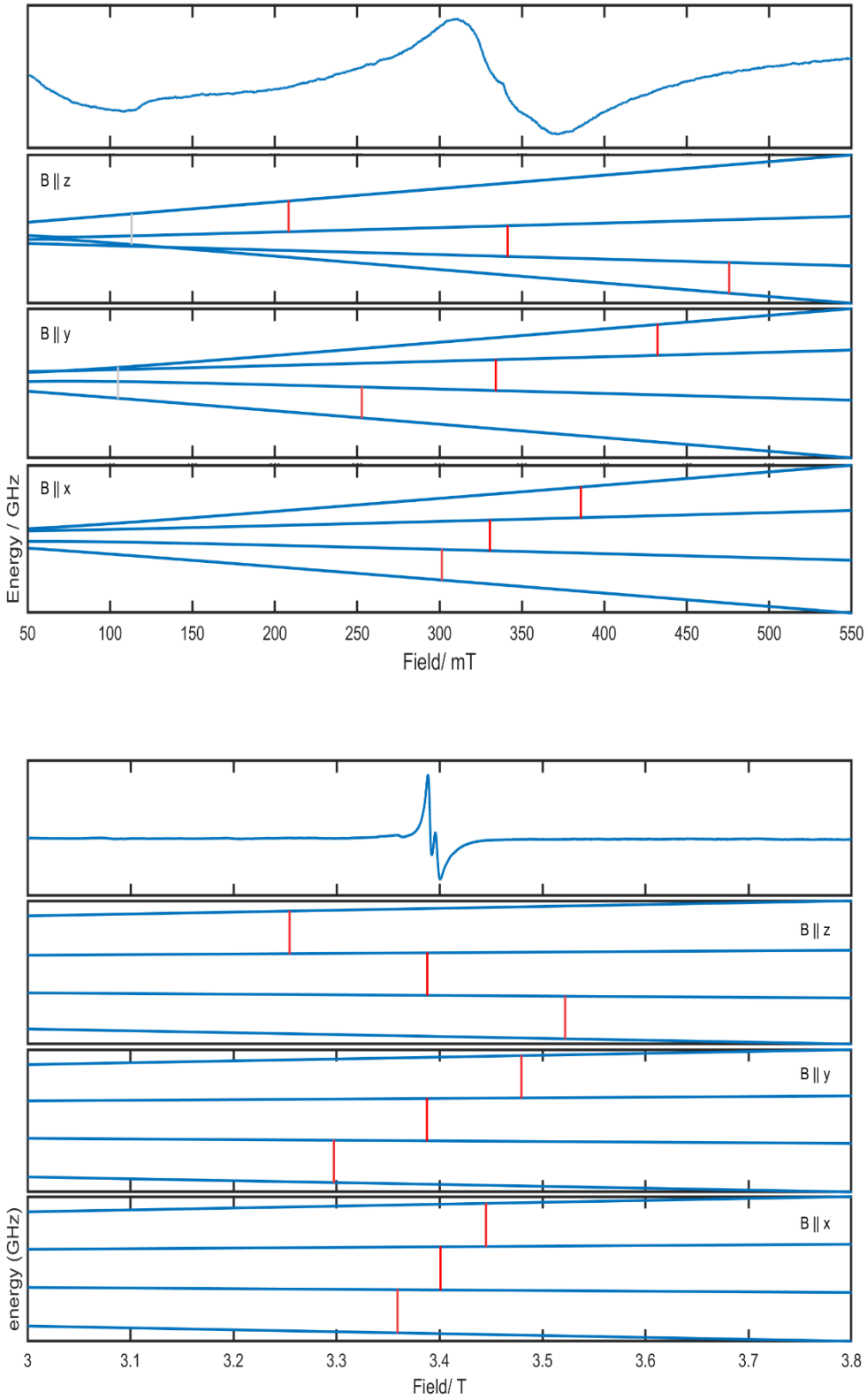

Figure S3 Energy level Zeeman diagram for [Cr(**bpi-1**)$_2$]PF_6 at 9.5 GHz (top) and 95 GHz (bottom), indicating the permitted (red) and forbidden (grey) transitions.

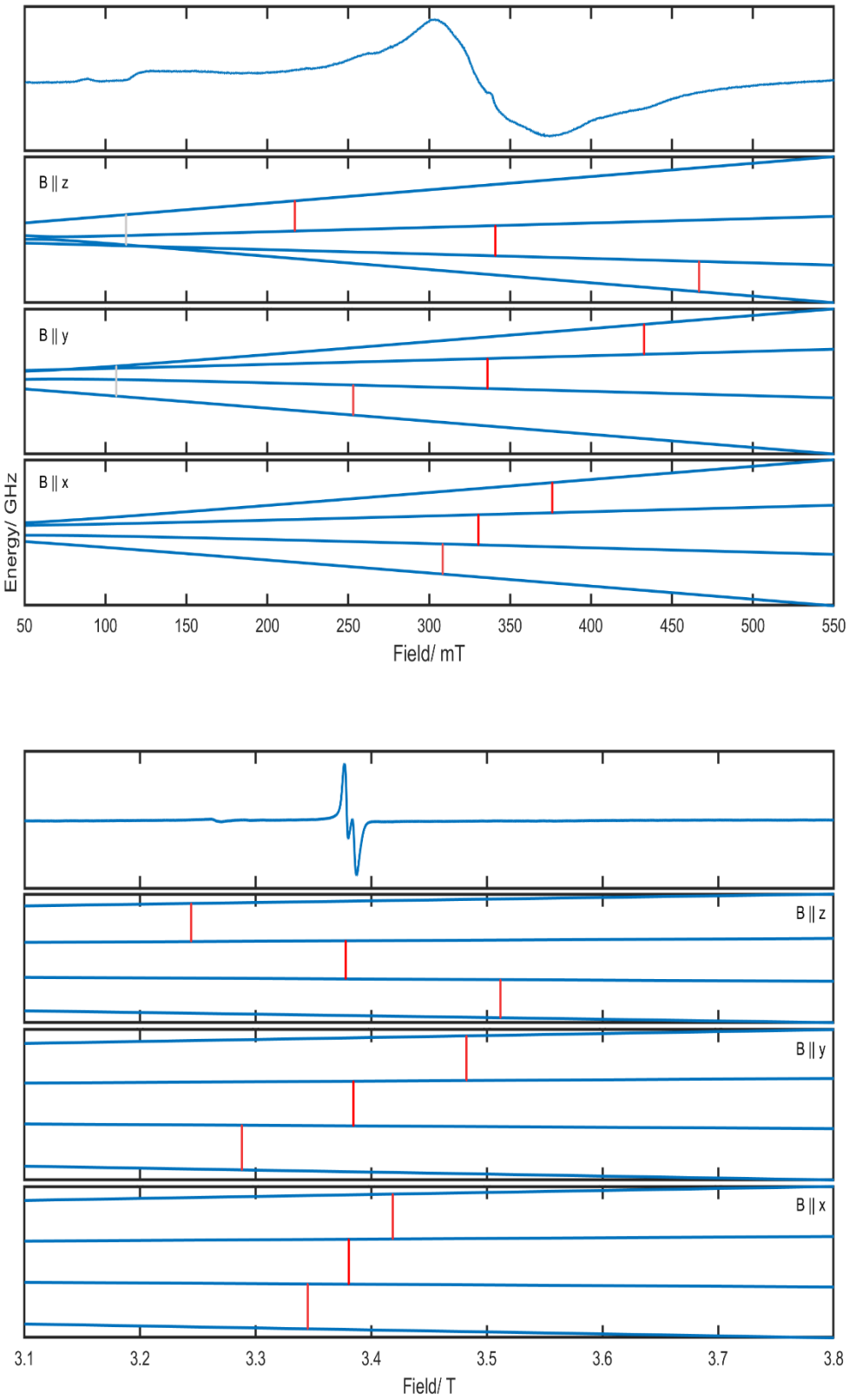

Figure S4 Energy level Zeeman diagram for [Cr(**bpi-2**)$_2$]PF$_6$ at 9.5 GHz (top) and 95 GHz (bottom), indicating the permitted (red) and forbidden (grey) transitions.

Table S4. A comparison of the spin Hamiltonian parameters for [Cr(**bpi**)$_2$]PF$_6$ against a series of literature Cr(III) complexes.

		g			D / cm^{-1}	E/D	Ref
		g_1	g_2	g_3			
[Cr(**bpi-1**)$_2$]PF$_6$	Expt	1.977	1.985	1.985	0.062	0.12	This work
	[a]DFT	1.986	1.989	1.990	0.061	0.261	
[Cr(**bpi-2**)$_2$]PF$_6$	Expt	1.980	1.986	1.987	0.062	0.15	
	DFT	1.986	1.989	1.990	0.024	0.324	
Cr(acac)$_3$					0.592	0.052	[6]
[Cr(bpy)$_2$(ox)]Cl		1.98	1.99	2.00	0.49	0.064	[7]
[Cr(phen)$_2$(ox)]Cl		1.989	1.983	1.988	0.398	0.124	
[Cr(salen)]Cl		1.96	1.96	1.97	0.70	0.063	[8]
[Cr(Jacobsen]Cl		1.95	1.95	1.95	0.80	0.108	
trans-[Cr(py)$_4$Cl$_2$]$^+$					0.164	0.001	[9]
[Cr(tpy)Cl$_3$][a]					0.034	0.010	[10]
mer-[CrCl$_3$(pzH)$_3$]		1.99	1.99	1.99	0.16		[11]
mer-[CrCl$_3$(4-Me-pzH)$_3$]		1.99	1.99	1.99	0.15		
mer-[CrCl$_3$(4-Cl-pzH)$_3$]		1.99	1.99	1.99	0.073		

a) Spin Hamiltonian calculations were performed on the geometry optimised ground state complexes, utilising B3LYP functional and def2-TZVPP (Cr atom) and EPR-II (C. N. O atoms) basis sets. For a detailed discussion of the optimum choice of DFT methods for calculation of spin Hamiltonian parameters of Cr(III) systems, the reader is referred to the works of Takui *et al*.,[6] and Misra *et al*. [12]. No evidence of ^{53}Cr or ^{14}N hyperfine coupling was observed experimentally at either X- or W-band, as anticipated based upon the small hyperfine couplings predicted via the DFT calculations:

$|A(^{53}Cr)|$ = [19.64 19.68 19.74] MHz, [$\alpha\beta\gamma$] = [6.03 1.69 5.78] rad

$|A(^{14}N)_{isoindoline}|$ = [4.27 4.50 4.86] MHz, [$\alpha\beta\gamma$] = [1.62 1.09 5.64] rad

$|A(^{14}N)_{py}|$ = [4.03 4.33 4.63] MHz, [$\alpha\beta\gamma$] = [5.90 0.83 2.83] rad

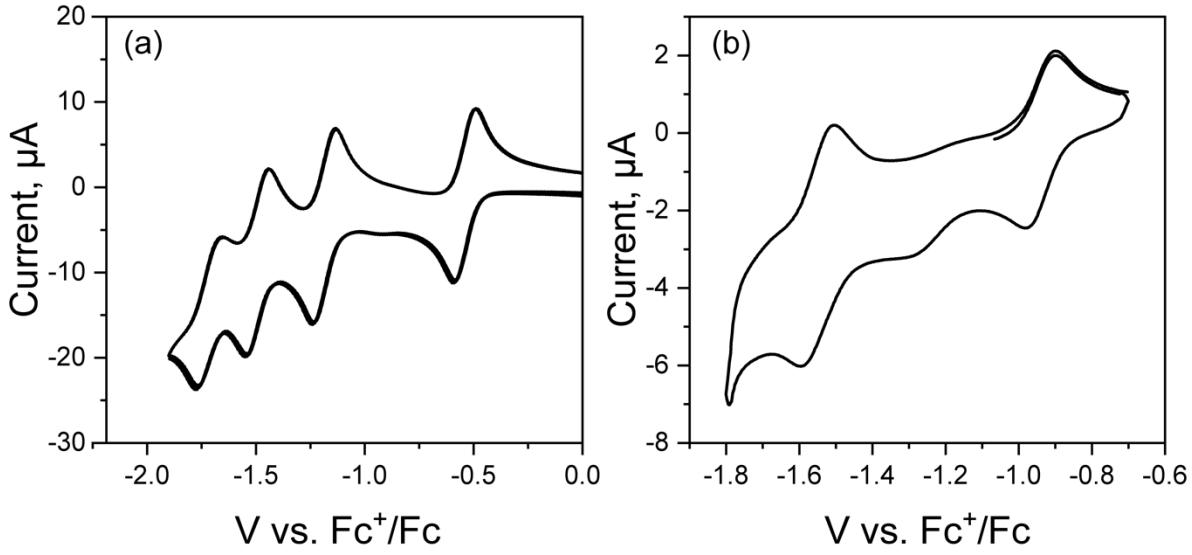

Figure S5 Cyclic voltammogram obtained for (a) [Cr(**bpi-1**)$_2$]PF_6 and (b) [Cr(**bpi-2**)$_2$]PF_6. De-oxygenated dichloromethane at a glassy carbon working electrode (scan rate 100 mV s^{-1}, 1×10^{-3} M solutions, 0.1 M [NBu_4][PF_6] as a supporting electrolyte).

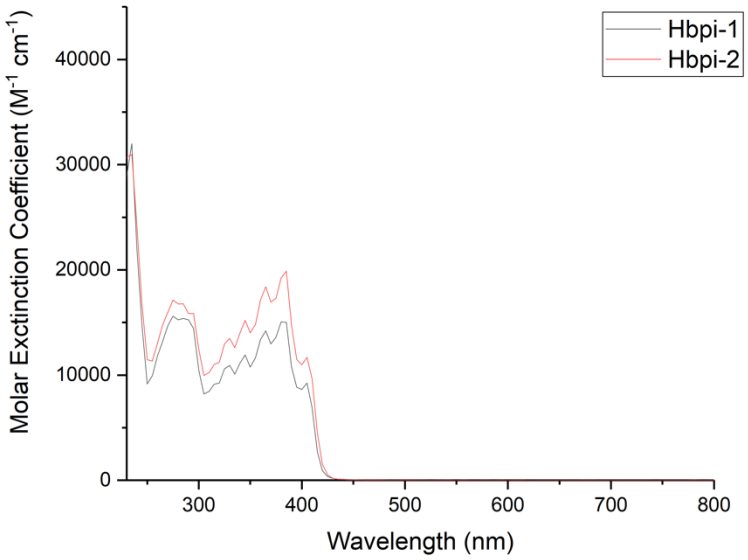

Figure S6 UV-vis. absorption spectra for the ligands **Hbpi-1** and **Hbpi-2** (MeCN).

Computational Calculations

Non-relativistic calculations of the fully relaxed geometries in the ground and excited states were performed on the Gaussian 09 program, and calculations of the spin Hamiltonian parameters were performed using ORCA (version 4.0.0.1). [13,14] Geometry optimisations were performed without constraints using the B3LYP functional and 6-31G(d,p) basis set for all atoms, excluding the Cr(III) centre for which the LANL2DZ basis set was applied. TD-DFT studies were performed using the same functional, but with Def2SVP on all atoms, and also included a simulated MeCN environment using the polarized continuum model (PCM) approach. For prediction of absorption spectra (n_{states} = 60), the geometry used to calculate orbital and other properties was used without modification.

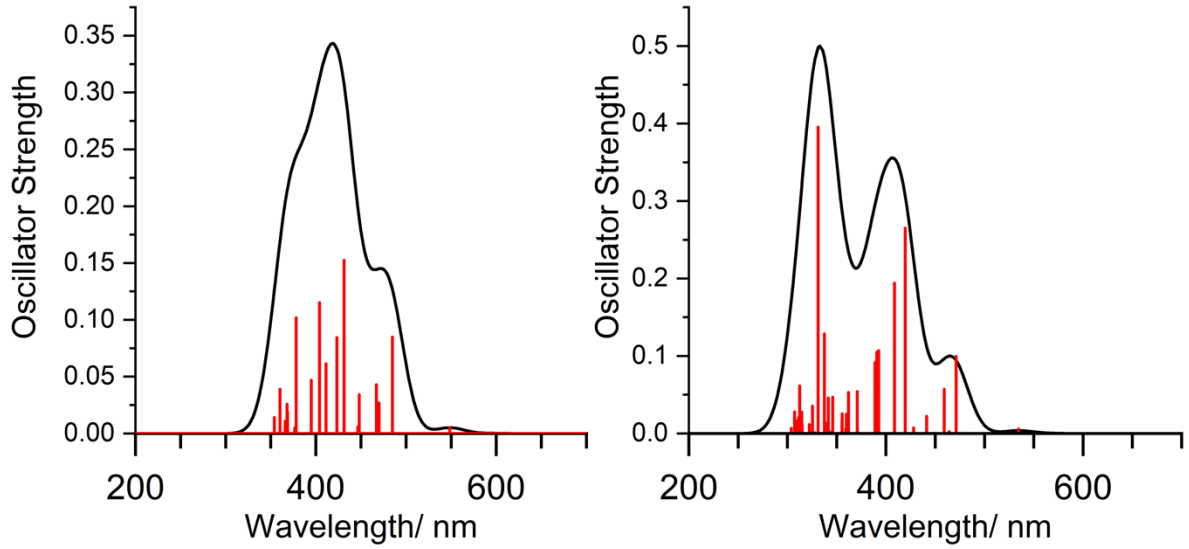

Figure S7 Calculated UV-Vis. absorption profiles for [Cr(**bpi-1**)$_2$]PF_6 (left) and [Cr(**bpi-2**)$_2$]PF_6. Calculated vertical transitions are shown in red (n_{states} = 60) and modulated with a Gaussian linewidth (default Gabedit settings applied to Gaussian convolution).

Note that no absorption bands were calculated above ~ 550 nm, despite observation of metal centred *d*–*d* transitions in the corresponding experimental spectra. Similar results were reported by Wenger *et al*.,[15] using identical computational methodologies. The absence of metal-centred transitions in the computational calculations are likely to arise from limitations in theoretical approximations embedded within the choice of functionals, and it is noted that the use of TD-DFT should be used

with caution when dealing with formally spin-forbidden *d*–*d* excitations of transition metal complexes, especially for high-spin systems.[16]

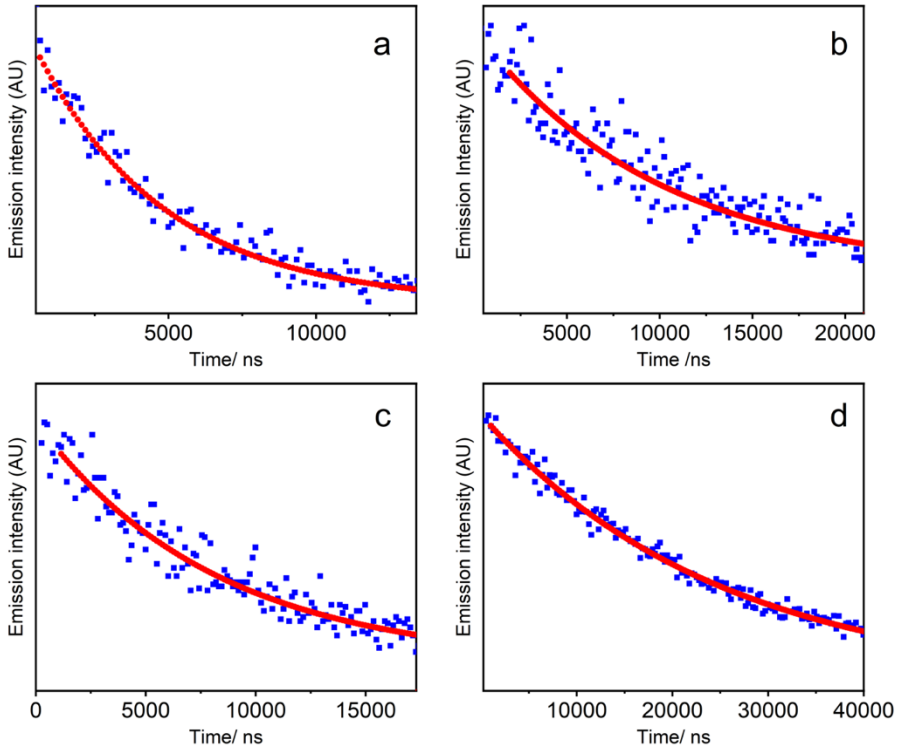

Figure S8 Emission lifetime data (λ_{ex} = 355 nm) for (a,b) [Cr(**bpi-1**)$_2$]PF_6 and (c,d) [Cr(**bpi-2**)$_2$]PF_6 recorded under aerated (a,c) and degassed (b,d) conditions.

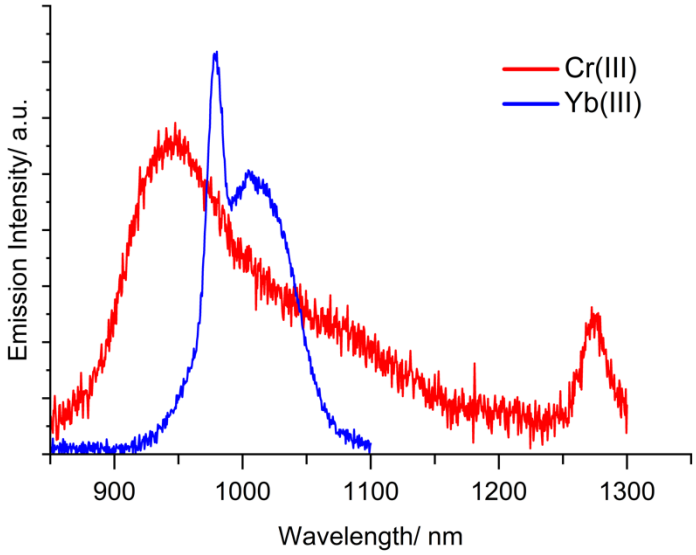

Figure S9 A comparison of the emission profiles for [Cr(**bpi-1**)$_2$]PF_6 and [Yb(TTA)$_3$(H_2O)$_2$] (where TTA = 3-(2-thenoyl)-1,1,1-trifluoroacetylacetonate) recorded under aerated solvent conditions.

References

1) CrysAlisPro Software System, Rigaku Oxford Diffraction, (2021).
2) G.M. Sheldrick, *Acta Cryst.*, 2015, **A71**, 3.
3) O.V. Dolomanov, L.J. Bourhis, R.J. Gildea, J.A.K. Howard, H. Puschmann, *J. Appl. Cryst.*, 2009, **42**, 339
4) G.M. Sheldrick, *Acta Cryst.*, 2015, **C27**, 3
5) S. Stoll, A. Schweiger, *J. Magn. Reson.*, 2006, **178**, 42.
6) K. Sugisaki, K. Toyota, K. Sato, D. Shiomi, T. Takui, *Phys. Chem. Chem. Phys.*, 2017, **19**, 30128
7) W. T. M. Andriessen, M. P. Groenewege, *Inorg. Chem.*, 1976, **15**, 621.
8) K. P. Bryliakov, M. V. Lobanova, E. P. Talsi, *J. Chem. Soc., Dalton Trans.,* 2002, 2263.
9) E. Pedersen, H. Toftlund, *Inorg. Chem.,* 1974, **13**, 1603.
10) S. K. Padhi, D. Saha, R. Sahu, J. Subramanian, V. Manivannan, *Polyhedron,* 2008, **27**, 1714.
11) J. M. López Plá, A. K. Boudalis, J. Telser, R. G. Raptis, *Inorg. Chim. Acta,* 2020, **502**, 119299.
12) T. Goswami, A. Misra, *J. Phys. Chem. A*, 2012, **116**, 5207.
13) F. Neese, *Wiley Interdiscip. Rev. Comput. Mol. Sci.*, 2012, **2**, 73.
14) F. Neese, *WIREs Comput. Mol. Sci.*, 2018, **8**, e1327.
15) N. Sinha, J.-R. Jiménez, B. Pfund, A. Prescimone, C. Piguet, O. S. Wenger, *Angew. Chem. Int. Ed.*, 2021, **60**, 23722.
16) F. Vlahović, M. Perić, M. Gruden-Pavlović, M. Zlatar, *J. Chem. Phys.*, 2015, **142**, 214111.